Materials Research. 2025; 28: e20240477
DOI: https://doi.org/10.1590/1980-5373-MR-2024-0477

Mechanical, Microstructure and Corrosion Properties of Friction Stir Welded Dissimilar Austenitic Stainless Steel Joints

Sundar raju Govindaraj*[a] , ***Senthil Vaithilingam*[b], *Sivakumar Karuppan*[a]**

[a]*Bannari Amman Institute of Technology, Department of Mechanical Engineering, Erode, Tamilnadu, India.*
[b]*Government college of Engineering, Department of Mechanical Engineering, Bodinayakkanur, Tamilnadu, India.*

Received: October 22, 2024; Revised: March 27, 2025; Accepted: April 21, 2025;

In many industries, challenges arise when welding dissimilar materials using traditional methods, such as fusion welding. These challenges often lead to problems like cracking, phase segregation, and intermetallic formation. To solve these issues, a low-operating-temperature friction stir welding (FSW) technique was employed to fabricate dissimilar stainless steel joints. In this study, AISI 304 and AISI 316 dissimilar butt joints were welded by friction stir welding at different tool rotational speeds of 600 to 900 rpm with a constant welding speed of 40 mm/min and an axial load of 15 kN. AISI 304 was on the retreating side, and AISI 316 was on the advancing side during the welding operation. At a tool rotation speed of 800 rpm, defect-free, dissimilar FSW joints with good mechanical characteristics were achieved. The tensile result indicates that the yield strength of the welded metal is higher than that of both base metals. Similarly, the hardness of the weld metal was higher than those of the base metal. It is due to the microstructural refinement of the weld metal attained by dynamic recrystallization caused by the stirring action of the tool at elevated temperatures. The microstructural results indicate ductile fracture properties. The pitting potential of dissimilar steel joints is less than that of similar AISI 304 and AISI 316 joints. However, it can stand in severe, corrosive environments.

Keywords: *Friction stir welding, Dissimilar, Tool rotational speed, Recrystallization, Corrosion.*

1. Introduction

A solid-state friction stir welding (FSW) technique was first invented by Wayne Thomas and E. Nicolas at the Welding Institute (TWI) of the UK in 1991[1]. It is a very efficient metal joining process due to the soundness of the weld, less energy consumption, and being environmentally friendly[2]. Filler wires are not needed in FSW which leads to reduced cost. In addition, butt-joints with high mechanical properties can be produced in Al-alloys by this solid-state joining technique compared to riveting, leading to considerable weight reduction in aerospace and automobile applications[3-8].

It has emerged and been established as an extremely effective alternative to traditional MIG welding for use in marine applications[9]. In fusion welding of stainless steels, heat-affected zones may be subjected to intergranular attack due to carbide precipitation caused by the welding thermal cycle[10-12]. Now, FSW will become a commercially attractive method for the fabrication of ships, pipes, trucks, railway wagons, and hot plates[13]. Both steels have an austenitic microstructure but AISI 316 is more resistant to corrosion due to the presence of molybdenum, which enhances resistance to pitting. AISI 304 and AISI 316 steel are generally suitable for welded cryogenic equipment in many corrosive environments[14]. FSW of dissimilar metals has many challenges when compared to welding of similar metals because of differences in physical, chemical, mechanical, and thermal properties[15-18].

During dissimilar friction stir welding (DFSW), material encounters several difficulties, such as precipitation of the detrimental intermetallic phases, grain coarsening, and solidification cracking[19]. In DFSW, parameters such as material position, tool offset, rotational speed, and traverse speed also significantly influence material flow, interfacial bonding, microstructure evaluation, and joint strength[20].

The tool rotational speed plays a major role in the amount of heat generation in the FSW process and can significantly impact the quality of the welding process. Ko et al.[21] found the tensile strength and hardness of the stir zone increased as the tool rotational speed increased. The higher tool rotational speed generates more frictional heat at the weld interface, causing the material to soften and become more malleable. However, most of these phenomena are qualitative, and the results are based on the resulting weld defects. So, optimal heat generation is essential for creating a defect-free weld.

The major problems involved in the FSW of steel alloys are the reduction in wear and corrosion resistance of the tool[22]. The quality and durability of the weld are directly influenced by the tool material. The material for the chosen tool must be able to withstand high temperatures and be durable against chemical and mechanical wear[23]. Because of the significant advancements made in FSW tool material, it is now possible to perform long welds in a variety of engineering steels with high quality[24]. Ragu Nathan et al.[25]

*e-mail: sunmetly@gmail.com
Associate Editor: José Daniel Biasoli de Mello.
Editor-in-Chief: Luiz Antonio Pessan.

investigated the deterioration of different tool materials in FSW, finding that among tungsten alloy tools, the one with 99%W and 1%La_2O_3 maintains good properties at high temperatures with negligible tool debris and base-material degradation. The same tool material was selected for performing welding in this experimental study. Marine structures and ships are continuously in contact with sand and silt, which can promote locally corrosive conditions[26]. About 18% chromium is added to grades AISI 304 and 316 to create this chromic film, and 2% molybdenum is added to 316 to further increase corrosion resistance. AISI 304 can be used for fully exposed components that are routinely cleansed with fresh water, whereas AISI 316 can be used for all hull and deck fitting applications above the water line[27]. These materials provide varying degrees of corrosion resistance and durability. For this reason, the research explores the effect of tool rotational speed on the mechanical, microstructural, and corrosion properties of dissimilar friction-stir welded AISI 304 and AISI 316 stainless steel using a W-La_2O_3 tool.

2. Experimental Procedure

The cold-rolled and annealed AISI 304 stainless steel-grade sheet with a thickness of 3mm was utilized as the base material. The operation employed a semi-automatic friction stir welding machine equipped with a Rexroth controller and a liquid-cooled tool holder machine. The machine had a spindle speed of 2000 rpm and a Z axial force of 15 kN. The technique utilized a cylindrical W alloy tool with a shoulder diameter of 25 mm, a probe diameter of 12 mm, and a conical pin length of 2.9 mm. To test the FSW joints, the tool's rotational speed was varied at 600, 700, 800, 900, and 1000 rpm, with a tool tilt angle of 0°, while maintaining a constant welding speed of 40 mm/min and an axial load of 15 kN.

X-ray film radiography produces images that are potentially useful for detecting volumetric defects. ASTM E1032-95 standards are followed to conduct this test. The UTM machine (M-30 model) under computer control was utilized to conduct experiments. The tensile specimens prepared as per ASTM E8M-04. A Charpy impact specimen ASTM E23-06 was followed. The impact toughness of the AIT-300-EN type samples was examined using an impact test machine with a 300 J capacity. The specimens were produced according to ASTM E190-03 specifications and tested in a compression testing machine with a load capacity of 400 kN. The Vickers micro hardness testing machine was used to conduct micro hardness tests on base metal, weld metal, and TMAZ with an applied load of 500 gf and a dwell time of 10 seconds. Figure 1 shows the OM micrograph and SEM micrographs of base metal AISI 304 and AISI 316.

The microstructure of the weld metal was examined using a computerized optical microscope and a high-resolution field emission scanning electron microscope (FESEM). X-ray diffraction (XRD) analysis was utilized to investigate the

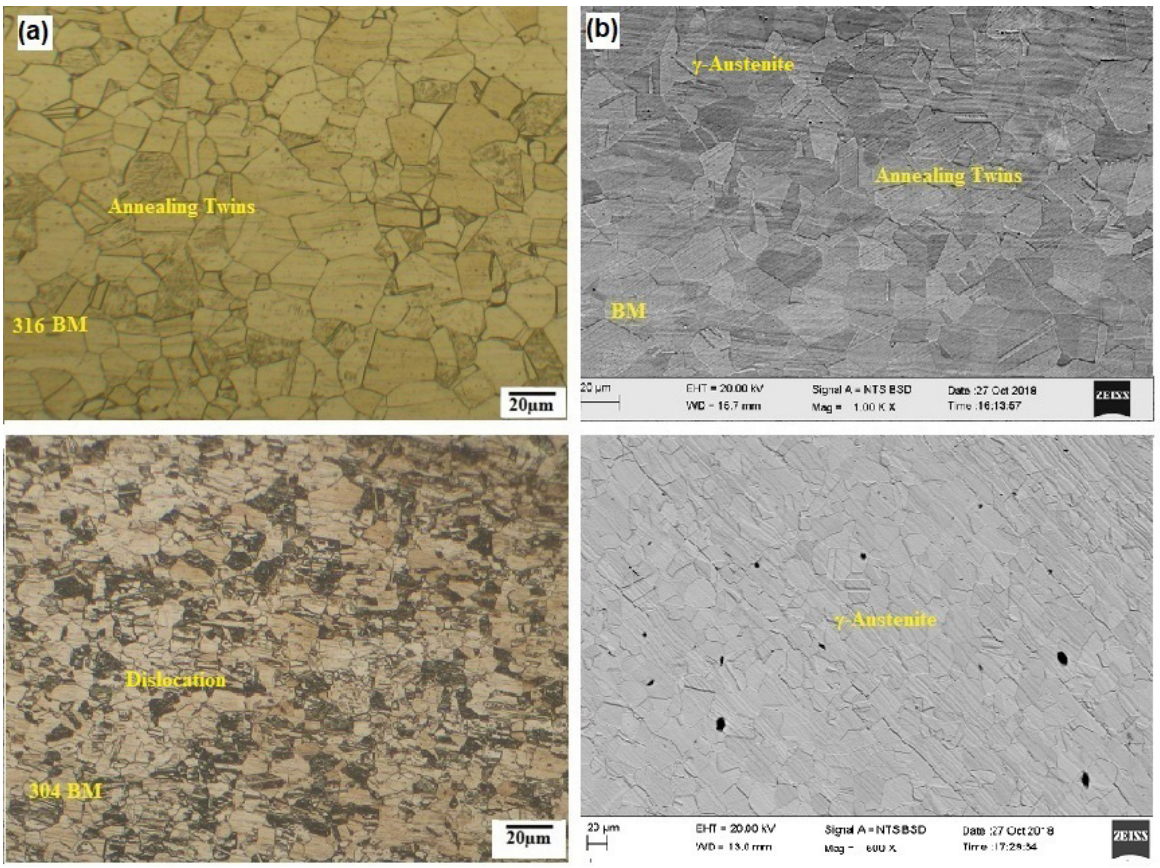

Figure 1. Microstructure of base metal AISI 304 &AISI 316 (a) OM micrograph (b) SEM micrograph

different phases present in the material. Tensile specimens were prepared according to ASTM E8M-04. ASTM G59-97 is utilized for the purpose of conducting corrosion testing. To perform a potentiostat corrosion test, a 3.5 percent NaCl solution and a three-electrode setup were employed. The working electrode in this test is the test specimen, while the reference electrode is calomel and the counter electrode is platinum. The corrosion test, manufactured by Gamry, was conducted with a scan rate of 1 mV/s and a voltage range of 0.5 V to +1.5 V. The exposed surface area in all experiments was 0.20 cm^2.

3. Result and Discussion

FSW joints were produced at different tool rotational speeds of 600, 700, 800, and 900 rpm at constant welding speed of 40 mm/min and axial load of 15 kN. The FSW process parameters and welding conditions are presented in Table 1.

Table 1. FSW process parameters and welding conditions.

Process parameters	Values
Tool rotational speed (rpm)	600, 700 ,800 & 900
Welding speed used (mm /min)	40
Axial force (kN)	15
Pin Length ,L (mm)	2.9
Tool Shoulder diameter, D (mm)	25
Pin diameter, d (mm)	6
Tool inclined angle (deg˚)	0
Tool material	W alloy (99% Tungsten & 1% of La_2O_3)
Base metal	AISI 304- AISI 316

The joint formed at a tool rotational speed of 600 mm/min shows weak consolidation, leading to weld nugget defect. It is due to the low temperature and inadequate material flow in the stir zone. The weld produced at 700 mm/min also exhibits a lack of bonding defect because of a low frictional force, which created insufficient heat input. At a tool rotational speed of 800 mm/min surface, volumetric defect-free weld joints are achieved. The smooth, onion-ring-like welds in the stir zone indicate appropriate heat generation during welding and adequate plastic flow of material. Finally, significant flash generation and tunnel defects are found at a tool rotational speed of 900 mm/min because of excessive heat input and the high tool shoulder pressure. The Figure 2 shows visual and X-ray Radiography inspection images of a FSW joints.

A visual inspection is performed to verify the surface quality and integrity of the weldments. Friction stir welds are assessed by X-ray radiography and visual inspection techniques. Post-weld inspection was conducted to check the surface quality of the completed weld joint. Figures 2a and 2b illustrate the face side and root side of the specimen welded at a tool rotational speed of 800 rpm. In Figure 2a, on the face side of the weld, no visible flaws on the surface and minimal flash were found at the side of the welding. Similarly, Figure 2b shows the root side of the weld surface, where the materials have been extensively sheared. The surface appearance of the face-side weld metal exhibits uniforms circular ripples. The rotation speed and transverse speed of the tool determine the pitch between the ripples. Initially, the width of the ripple is small due to the low frictional temperature, but the majority of the weld metal shows uniform-width ripples at the same tool rotational speed.

In Figure 2c, an X-ray film image of the weld joint produced at a tool rotational speed of 800 rpm is depicted.

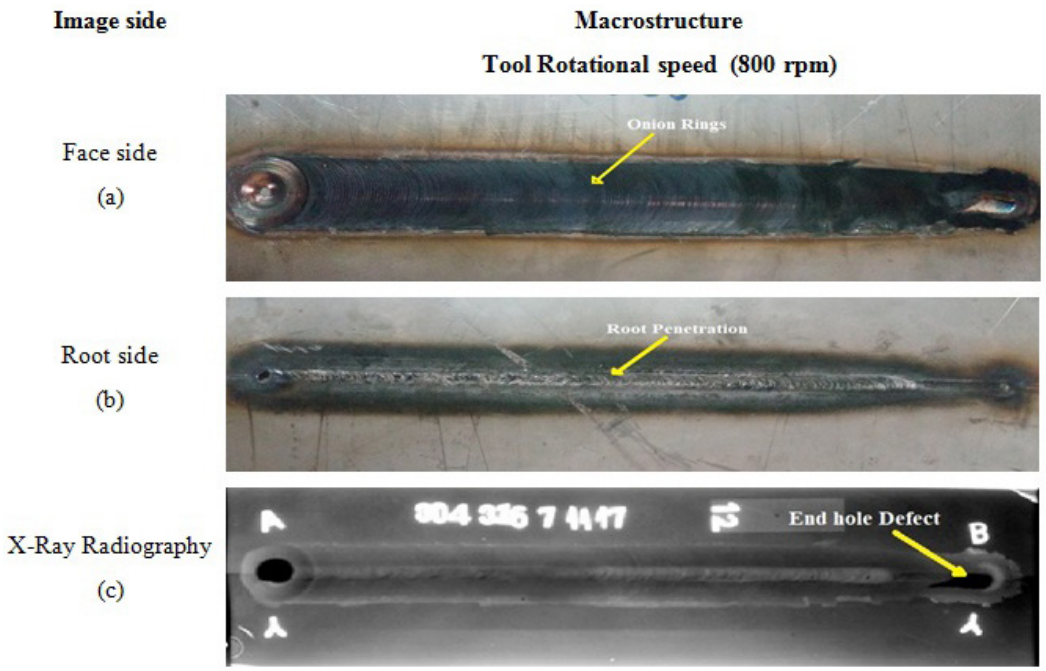

Figure 2. Visual inspection and X-ray radiography images of a FSW joints.

The result indicates that the welds do not have any internal micro-defects or root-side defects, which can be attributed to good material flow ability due to optimal heat energy. It implies that the welds were homogeneous and of sound quality. However, a keyhole defect was observed in the work piece at the point of retraction. This exit hole can be repaired using an active passing filling friction stir repair technique.

3.1. Mechanical testing

3.1.1. Tensile test

Figure 3 shows the transverse tensile properties of the BM and FSW joints. The experimental result shows that the yield strength (YS) and ultimate tensile strength (UTS) of the AISI 304 base metal are 343 MPa and 674 MPa, and the AISI316 base metal is 310 MPa and 608 MPa. With the tool rotational speed of 800rpm, the dissimilar joint yield strength is higher than both base metals. The average of three weld specimen yield strength (YS) is estimated at 374 MPa due to continuous grain refinement and work hardening effect in the weld zone. The 304 and 316 base metals had higher ductility than the steel because all austenitic stainless steel has abundant ductility when annealed. The high-yield strength steels are the preferred material to work under incredible load stresses.

At a tool rotational speed of 800 rpm the ultimate tensile strength was measured at 587Mpa, which is lower than both base metals. It is due to poor material coalescence and non-homogeneity of interface region reducing the strength of the joint. The location of the fracture was observed in the stir zone. Jafarzadegan et al.[28] also experienced a similar result in the welding of austenitic stainless steel and low-carbon steel. The FSW sample had higher yield strength than base metal due to smaller grains increasing the yield strength according to the Hall-Petch relationship. The 304 and 316 steel base metals had 63% and 57% elongation respectively. The elongation of the weld was 34% less than the elongation of base metals because of considerable grain refining in the weld area. In fine-grained steel, the limited elongation with a decrease in grain size is due to necking occurring at the early stage of the tensile test.

3.1.2. Impact test

Room temperature Charpy V-notch impact test results show the base metal 304 and 316 impact toughness values are 64 J and 50 J respectively. The weld metal average toughness value obtained 40 J at a tool rotational speed of 800 rpm. The impact toughness of the welds was lower than the base metal. It may be severe tool wear during dissimilar welding and migration of tungsten particles from the tool to the weld stir zone. It acts as a secondary phase particle inclusion and stress raiser to reduce the toughness of the metal. As Tiwari et al.[29] reported, tool wear is common in the FSW of hard alloy material. It is a combination of chemical and mechanical wear mechanisms that occur in high welding temperature and stress conditions. During welding fine grained tungsten particles are converted into coarse grains due to the weld thermal cycle. Figure 4 Shows the Charpy V-Notch impact test result.

3.1.3. Bend test

The compressive strength evaluations of the welded joints have been carried out using a three-point guided bend test. The specimens were subjected to a bending load in both face bend and root bend configuration such that the face and root samples' outer surfaces changed into a U-shape. During the test, the weld zone surface is highly stressed in tension, and any flaw or lack of fusion will open up due to the high tensile stress. The test specimens are extracted from the transverse direction of the weld coupon. All specimens were examined for defects at the outer surface using visual inspection, and there were no cracks or defects in the specimens.

The compressive strengths of the base metals 304 and 316 are measured at 53.7 MPa and 34.5 MPa, respectively. The weld metal strength observed at the face side was 45.5 MPa, and the root side was 53.4 MPa. The face-side ductility is between two base metals, and the root-side value is almost equal to the 316 base metal value. It is characterized

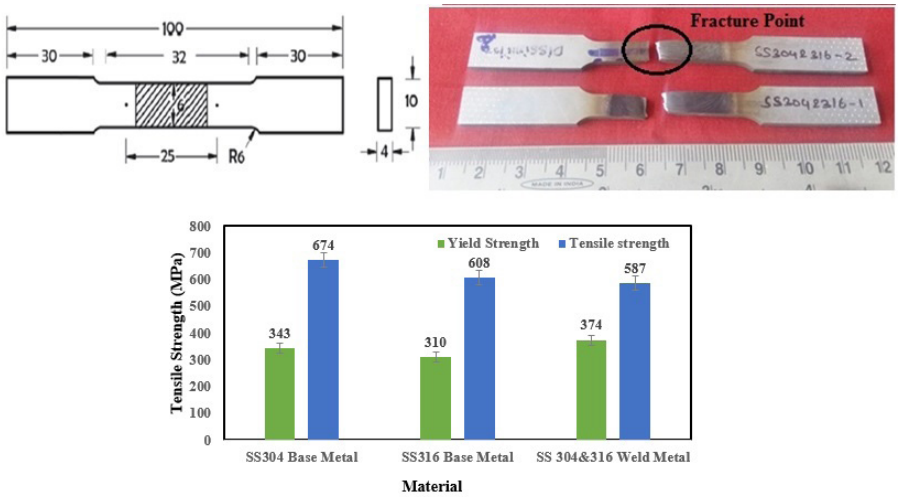

Figure 3. Transverse tensile properties of base metal and FSW joints.

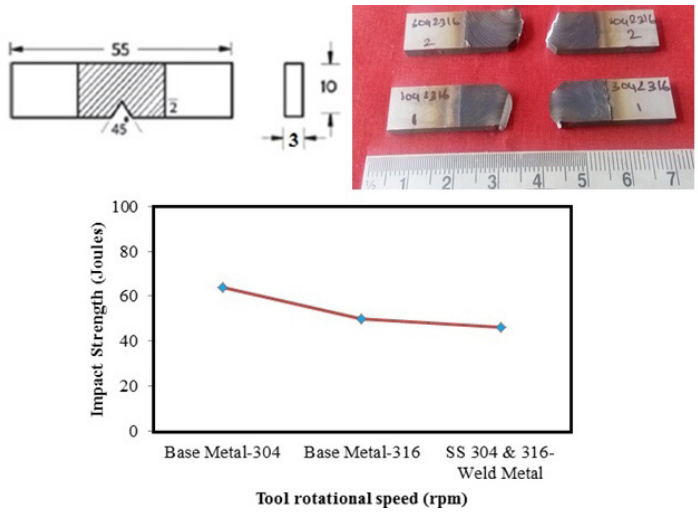

Figure 4. Charpy V-Notch impact test results.

by strong metal coalescence and good ductility at the face and root sides. As Das and Toppo[30] pointed out, it is due to the diffusion of the alloying components and sufficient mixing of two alloys. This dissimilar metal joint possesses the required ductility and qualifies as per the requirements of the ASME SEC IX standard. Figure 5 Compressive strength evaluations of welded joints.

3.1.4. Micro hardness test

AISI 304 and AISI 316 joint microhardness samples were extracted from the center of the weld in the transverse direction. During welding, a 304 plate is located on the advancing side, and a 316 plate is positioned on the retreating side. The hardness was measured from the 316 steel retreating sides to the 304 steel advancing sides. The microstructure and hardness profile confirmed that the dissimilar plate had different zones containing base metal, TMAZ, and stir zones. The obtained hardness profile is shown in the Figure 6.

The average base metal microhardness values of AISI 304 and AISI 316 were determined at 223±5HV and 185±5HV, respectively. The TMAZ of 316 steel hardness increases slightly above the base metal value due to partial or full grain refinement in the zone. The stir zone is composed of two different steels with different hardness. The hardness of the stir zone varies from 210 HV to a peak hardness of 252 HV in the centerline, and the average hardness is measured at 230±5 HV. As Danlolos and Pantelis[31] also proposed, this is expected because the dissimilar weld nugget consisted of a mixture of two-parent materials with a great difference in strength and hardness. In the stir zone, hardness values are increased when compared to the base metal due to refined grain structure and some features of dynamic recrystallization. Similarly, TMAZ values also slightly increased because of dynamic recovery. According to the Hall-Petch hardness relationship, the finer grains in the stir zone increase the hardness of the stir zone. The stir zone's higher hardness is due to the higher dislocation density in the austenitic grains and continuous dynamic recrystallization.

3.2. Metallurgical analysis

3.2.1. Microstructure

The microstructure of AISI 304 and AISI 316 stainless steel is mainly composed of austenite (Ɣ-Fe) under the condition of equilibrium solidification. The base material contains austenite grains with annealing twins created by the cold rolling heat-treatment process. The welded metal metallographic contains three different zones base metal, TMAZ, and stir zone. The microstructural study exposes the quality of the weld joint. It is due to fact that the mechanical properties of welded joints strongly depend on the microstructure of the joints, as also pointed out by Yan et al.[32].

The optical micrograph image of several regions of the friction stir-welded 304 and 316 joints is shown in Figure 7. The stir zone roughly shows an equiaxed grain structure. The dislocation density in the SZ is slightly higher than that in the BM. The microstructure in Figure 7a and 7b shows the SZ of the shoulder and pin-influenced regions. The finely equiaxed grains are observed throughout the SZ. Further, no annealing twin grains are found in the SZ, which is completely re-oriented by the stirring action of the tool. It is noted that the grain size decreases gradually from the top surface to the bottom surface of the weld joint due to the high peak temperature and slower cooling rate. The grain size in the stir zone is much smaller than in the base material due to the discontinuous recrystallization process (DRX).

The TMAZ is formed by the simultaneous effects of thermal and mechanical loads. The process is thermomechanical, with the material undergoing dynamic recrystallization (DRX) due to the interplay of temperature, strain, and strain rate. The combination of high rotational speed and tool pressure induces severe plastic deformation, breaking down the original grain structure. The microstructures in Figure 7c and 7d display the TMAZs of advancing and retreating sides. The image shows that the advancing side experiences the most

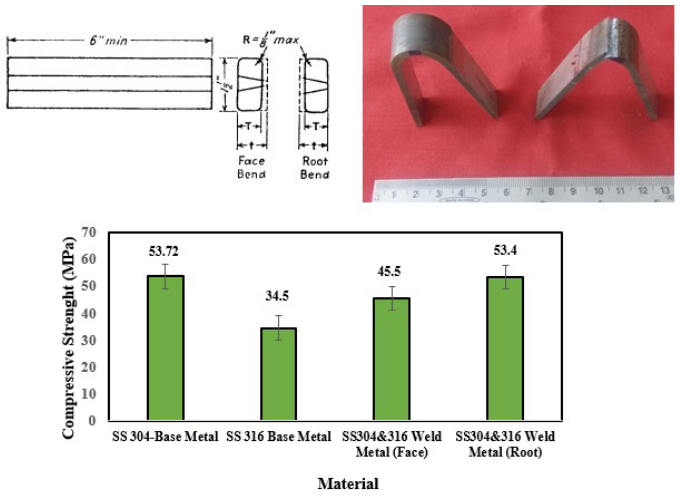

Figure 5. Compressive strength evaluation of welded joints.

severe deformation because of the material flow mechanism. Further, the sheer force of the advancing side of the tool induces a larger plastic deformation than the retreating side. It is observed that both advancing and retreating side grain structures have a high density of sub-boundaries and dislocations. The grain structure of TMAZ is bigger than that of SZ due to the dynamic recovery of the grains. The microstructure in Figure 7e and 7f depicts the SZ and TMAZ interface regions of the advancing and retreating sides. Compared to the TMAZ-AS and RS shoulder-influenced region and pin-influenced region, the size of the TMAZ zone is reduced near the bottom of the pin-influenced region due to a faster cooling rate. Normally, the FSW process heat is generated between the tool and the interface of the material surface. A large amount of heat is generated on the top surface. At the bottom TMAZ, the plating rate of heat dissipation is faster than the top surface. Park et al.[33] Moreover, the microstructure characteristics are roughly identical to friction stir-welded 2 mm-thick AISI 304 austenitic stainless steel.

3.2.2. Fracture surface analysis-a tensile test

The tensile specimen fracture surface of the base metal is shown in Figure 8a. The displayed fractography invariably consists of dimple dominant with a large void volume fraction. Generally, ductile failure often originates from the initiation, growth, and coalescence of microscopic voids during plastic deformation. The photographs show small, large dimples and micro voids. Noell et al.[34] which are an indication that the tensile specimens failed in a ductile manner under the action of uniaxial tensile loading. The tensile specimen fracture surface of welded metal is shown in Figure 8b. The exposed fractography is perceived to have a large amount of small and big dimples and micro-voids. The SEM morphology of the weldment fracture structure shows micro-voids and dimples, which are signs of ductile fracture. Compared to the base metal and weld metal fractography, fine-size dimples are observed in the weld metal. Furthermore, parabolic-shaped fine micro voids are present in the welded fracture

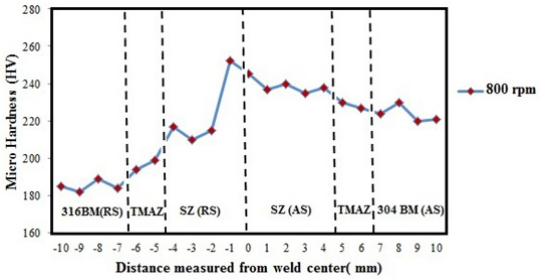

Figure 6. Microhardness survey results.

surface. It is a sign of optimum material flow, and plastic deformation occurs in the welded metal.

Figure 8c depicts the tensile test SEM-EDS analysis of base metal used to analyze the energy spectrum to determine the specific elements. Figure 8d shows the tensile test EDS analysis of weld metal. Generally, in the FSW process, light etching features occur between the tool and base material. These features are due to mechanical mixing and wear of tool material with base material under high pressure. In the shown EDS photograph, it is observed that no substantial W tool debris inclusion occurs in the weld joints. Since there is no shape change, no plastic deformation is witnessed in the tool pin. The tool debris is due to physical wear during welding.

3.2.3. Fracture surface analysis-an impact test

Figure 9a and 9b illustrate the typical SEM fractography of impact test images of base metal and weld metal. The fracture surface of impact specimens of base metal is shown in Figure 9a. The displayed fractography observed a fibrous appearance and large deformation before fracture, which indicates the properties of ductile shear fracture. Dada[35]. Further, the void coalescence results in the development of a shear lip, and the micro voids are responsible for higher upper self-energy fracture. Figure 9b illustrates the typical SEM fractography of impact test images of a welded joint. The exposed fractography witnessed micro voids and non-

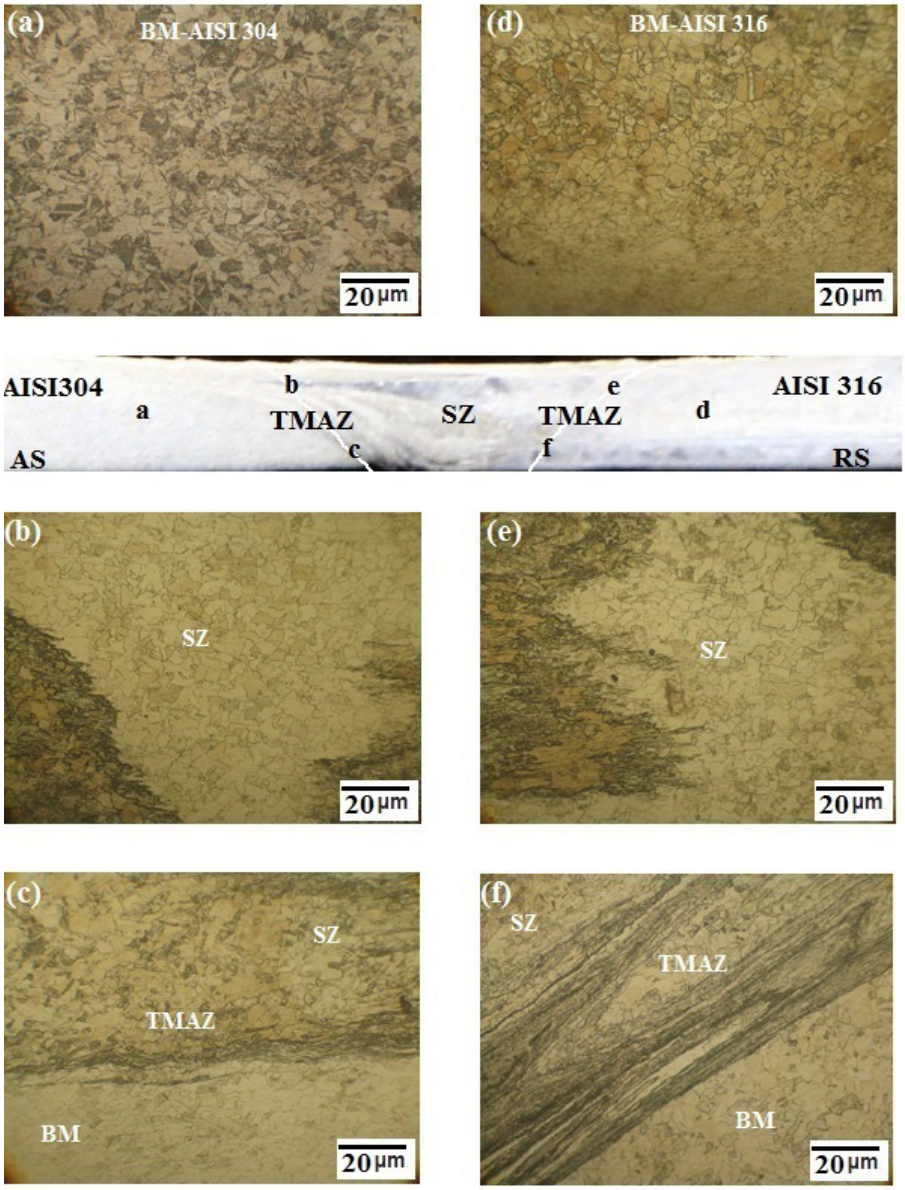

Figure 7. Optical micrographs of FSW joint regions- (a) BM–AISI 304, (b) SZ–Shoulder (AS-Top), (c) SZ–Pin (AS-Bottom), (d) BM–AISI 316, (e) SZ–Shoulder (RS-Top), (f) SZ–Pin (RS-Bottom).

uniform dimples, which are signs of a high-energy mode of ductile fracture. Inside the dimples, there is also shear cleavage and minor broken grains. The grains and void size also increased predominantly when compared to the base metal. It is the origin of the poor toughness of the material. Figure 9c depicts the SEM-EDS analysis of base metal. The result perceived in base metals Ni and Mn predominantly present after the Cr content is that they act as an austenite stabilizer. Figure 9d depicts the SEM-EDS analysis of weld metal. The result explains the composition of the weld metal in the fracture area. It is observed that the least amount of tungsten inclusion is present in the weld metal, which is the reason for the reduced toughness of the weld metal. However, a sufficient amount of toughness and tensile strength is attained at a welding speed of 800 rpm.

3.3. Corrosion testing

3.3.1. Pitting corrosion

Akpanyung and Loto[36] In a chloride environment, pitting corrosion is a mild, localized form of corrosion that can cause extremely destructive damage to structural elements like stainless steel. The potentiodynamic polarization test was performed to analyze the corrosion behavior of AISI 304-316 dissimilar friction stir-welded butt joints. The corrosion potential (E corr), corrosion current density (I corr), and pitting potential (E pit) of the welded metal were measured and compared with AISI 304 and AISI 316 base metal joints, as presented in Table 2. Potentiodynamic polarization Tafel curves of dissimilar welded metal joints are shown in Figure 10.

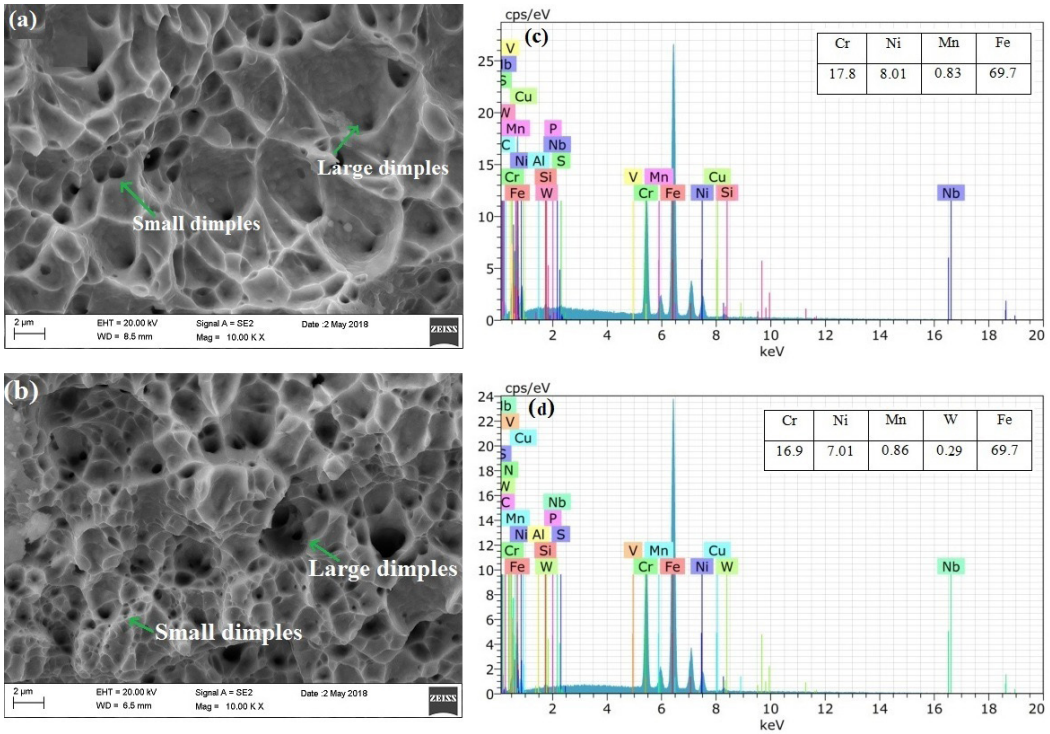

Figure 8. Tensile test- (a, b) Fractographs of base metal and weld metal (c, d) SEM-EDS base metal and weld metal.

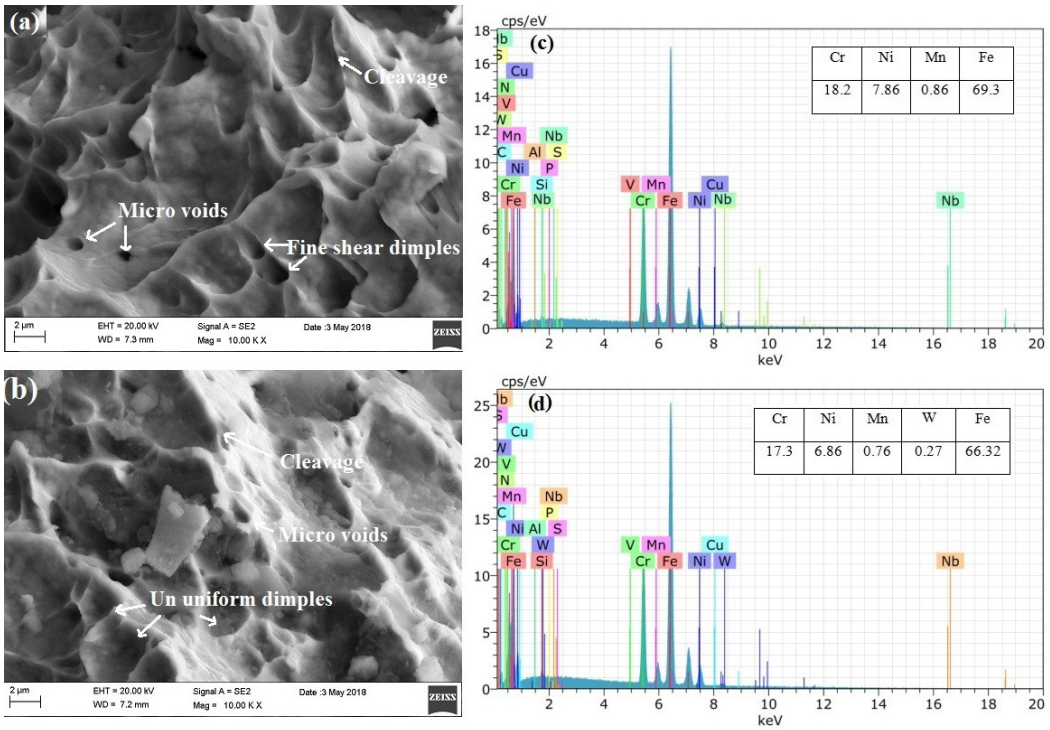

Figure 9. Impact test- (a, b) Fractographs of base metal and weld metal, (c,d) SEM-EDS base metal and weld metal.

The corrosion potential (E corr) values of AISI 304-316 dissimilar welded metals are 0.1402314 mV. Corrosion current density (I corr) values are kept constant at 0.000001 mA/cm2. The value of pitting (E pit) of 194 mV is observed in the dissimilar joint. Yi et al.[37] the results showed that the critical pitting potential (Epit) strongly depends on the scan rate. Compared to similar and dissimilar weld pitting potential, less value is found in AISI 304-316 joints. It is due to the

Table 2. Potentiodynamic polarization test results of base metal and AISI 304-316 welded joint.

Sample details	Corrosion Potential (E corr) mV	Corrosion current (I corr) mA/cm2	Pitting Potential (E pit) mv
AISI 304	-0.2373949	0.000001	210
AISI 316	-0.1577983	0.000001	258
AISI 304- 316	-0.1402314	0.000001	195

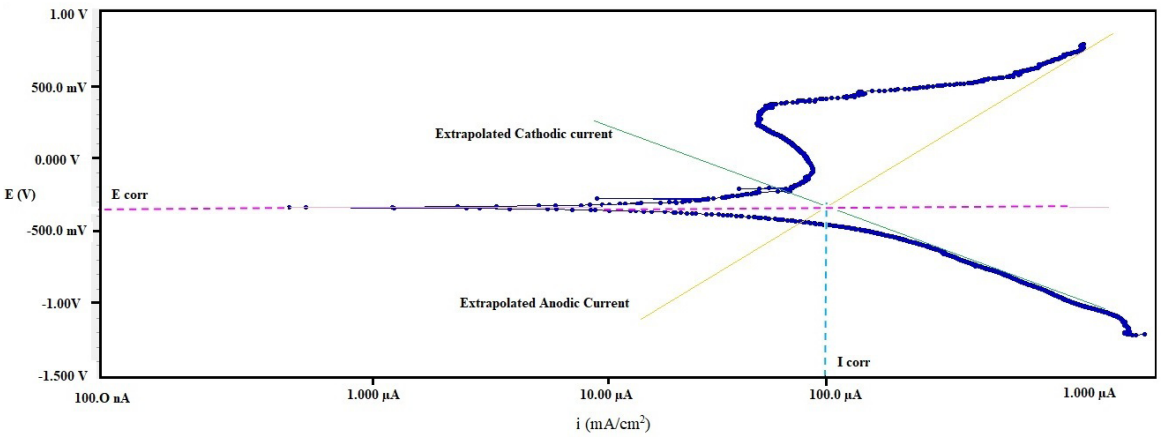

Figure 10. AISI 304- 316 weld metal potentiodynamic polarization Tafel curve.

two metal phases having different corrosion potentials that form an active-passive region and promote pitting corrosion. The dissimilar metal's corroded surface is witnessed with shallow and wider pits and micro channels. The test results identified that the pitting potential of dissimilar metals is less than that of similar AISI 304 and AISI 316 joints. However, it can stand in severe, corrosive environments.

4. Conclusion

The main conclusions of this study are as follows

- AISI 304 and AISI 316 dissimilar Austenitic stainless steel welded joints were successfully achieved using the friction stir welding process with an axial load of 15kN, a constant welding speed of 40 mm/min, and a tool rotation speed of 800 rpm.
- X-ray results indicate that the welds do not have any internal micro-defects or root-side defects, attributed to the optimal heat energy facilitating good material flowability.
- Studies showed that mechanical properties were directly influenced by welding process parameters, with a maximum tensile strength of 587 MPa and a compressive strength of 51 MPa obtained at a welding speed of 800 rpm.
- The impact toughness of the weld is slightly reduced, which could be attributed to severe tool wear during dissimilar welding and the migration of tungsten debris from the tool to the weld stir zone.
- The stir zone's micro-hardness was observed at a maximum of 230±5 HV due to the microstructural refinement of the weld metal achieved by dynamic recrystallization caused by the stirring action of the tool at elevated temperatures.
- The SEM image depicts the size and distribution of dimples in the tensile-welded specimen, indicating ductile fracture properties.
- Potentiodynamic polarization test results show E corr values of AISI 304-316 dissimilar welded metal at 0.1402314 mV. Corrosion current density (I corr) values are kept constant at 0.000001 mA/cm2. The pitting potential of dissimilar metals is less than that of similar AISI 304 and AISI 316 joints. However, it can withstand severe corrosive environments.
- FSW offers new ways to solve traditional joining problems. Many flaws associated with traditional fusion welding processes, including shrinkage, solidification cracking, and porosity, are eliminated with FSW.

5. References

1. Mishra RS, Ma ZY. Friction stir welding and processing. Mater Sci Eng Rep. 2005;50(1-2):1-78. http://doi.org/10.1016/j.mser.2005.07.001.
2. Kumar Rajak D, Pagar DD, Menezes PL, Eyvazian A. Friction-based welding processes: friction welding and friction stir welding. J Adhes Sci Technol. 2020;34(24):2613-37. http://doi.org/10.1080/01694243.2020.1780716.
3. Padhy GK, Wu CS, Gao S. Friction stir based welding and processing technologies-processes, parameters, microstructures and applications: a review. J Mater Sci Technol. 2018;34(1):1-38. http://doi.org/10.1016/j.jmst.2017.11.029.
4. Lukin VI, Erasov VS, Panteleev MD, Avtaev VV, Samorukov ML, Kulik VI. Friction stir welding of aircraft wings. Weld Int.

2018;32(10):690-4. http://doi.org/10.1080/09507116.2017.1398914.
5. Ahmed MMZ, El-Sayed Seleman MM, Fydrych D, Cam G. Friction stir welding in the aerospace industry: the current progress and state-of-the-art review. Materials. 2023;16(8):2971. http://doi.org/10.3390/ma16082971.
6. Kashaev N, Ventzke V, Cam G. Prospects of laser beam welding and friction stir welding processes for aluminum airframe structural applications. J Manuf Process. 2018;36:571-600. http://doi.org/10.1016/j.jmapro.2018.10.005.
7. Çam G, Ipekoglu G. Recent developments in joining of aluminium alloys. Int J Adv Manuf Technol. 2017;91(5-8):1851-66. http://doi.org/10.1007/s00170-016-9861-0.
8. Tang Y, Li W, Zou Y, Wang W, Xu Y, Vairis A, et al. Effects of tool rotation direction on microstructure and mechanical properties of 6061 aluminum alloy joints by the synergistically double-sided friction stir welding. J Manuf Process. 2024;126:109-23. http://doi.org/10.1016/j.jmapro.2024.07.067.
9. Martin J, Wei S. Friction stir welding technology for marine applications. In: Mishra RS, Mahoney MW, Sato Y, Hovanski Y, editors. Friction stir welding and processing VIII. Cham: Springer; 2015. https://doi.org/10.1007/978-3-319-48173-9_24.
10. Şenol M, Çam G. Investigation into microstructures and properties of AISI 430 ferritic steel butt joints fabricated by GMAW. Int J Press Vessels Piping. 2023;202:104926. http://doi.org/10.1016/j.ijpvp.2023.104926.
11. Serindağ HT, Cam G. Microstructure and mechanical properties of gas metal arc welded AISI 430/AISI 304 dissimilar stainless steels butt joints. J Phys Conf Ser. 2021;1777(1):012047. http://doi.org/10.1088/1742-6596/1777/1/012047.
12. Serindağ HT, Cam G. Multi-pass butt welding of thick AISI 316L plates by gas tungsten arc welding: microstructural and mechanical characterization. Int J Press Vessels Piping. 2022;200:104842. http://doi.org/10.1016/j.ijpvp.2022.104842.
13. Bhadeshia H, DebRoy T. Critical assessment: friction stir welding of steels. Sci Technol Weld Join. 2009;14(3):193-6. http://doi.org/10.1179/136217109X421300.
14. Teels STS. Materials for cryogenic service: engineering properties of austenitic stainless steels. Toronto: Nickel Dev Inst; 1974.
15. DebRoy T, Bhadeshia HKDH. Friction stir welding of dissimilar alloys: a perspective. Sci Technol Weld Join. 2010;15(4):266-70. http://doi.org/10.1179/174329310X12726496072400.
16. Ahmed MMZ, El-Sayed Seleman MM, Fydrych D, Cam G. Review on friction stir welding of dissimilar magnesium and aluminum alloys: scientometric analysis and strategies for achieving high-quality joints. J Magnes Alloy. 2023;11(11):4082-127. http://doi.org/10.1016/j.jma.2023.09.039.
17. Khaliq UA, Muhamad MR, Yusof F, Ibrahim S, Mohd Isa MS, Chen Z, et al. A review on friction stir butt welding of aluminum with magnesium: A new insight on joining mechanisms by interfacial enhancement. J Mater Res Technol. 2023;27:4595-624. http://doi.org/10.1016/j.jmrt.2023.10.158.
18. Çam G, Javaheri V, Heidarzadeh A. Advances in FSW and FSSW of dissimilar Al-alloy plates. J Adhes Sci Technol. 2023;37(2):162-94. http://doi.org/10.1080/01694243.2022.2028073.
19. Fu B, Qin G, Li F, Meng X, Zhang J, Wu C. Friction stir welding process of dissimilar metals of 6061-T6 aluminium alloy to AZ31B magnesium alloy. J Mater Process Technol. 2015;218:38-47. http://doi.org/10.1016/j.jmatprotec.2014.11.039.
20. ShivaKumar GN, Rajamurugan G. Friction stir welding of dissimilar alloy combinations: a review. Proc Inst Mech Eng, C J Mech Eng Sci. 2022;236(12):6688-705. http://doi.org/10.1177/09544062211069292.
21. Ko Y, Lee K, Baik K. Effect of tool rotational speed on mechanical properties and microstructure of friction stir welding joints within Ti–6Al–4V alloy sheets. Adv Mech Eng. 2017;9(8). http://doi.org/10.1177/1687814017709702.
22. Park SHC, Sato YS, Kokawa H, Okamoto K, Hirano S, Inagaki M. Microstructural characterisation of stir zone containing residual ferrite in friction stir welded 304 austenitic stainless steel. Sci Technol Weld Join. 2005;10(5):550-6. http://doi.org/10.1179/174329305X46691.
23. De A, Bhadeshia H, DebRoy T. Friction stir welding of mild steel: tool durability and steel microstructure. Mater Sci Technol. 2014;30(9):1050-6. http://doi.org/10.1179/1743284714Y.0000000534.
24. Liu FC, Hovanski Y, Miles MP, Sorensen CD, Nelson TW. A review of friction stir welding of steels: Tool, material flow, microstructure, and properties. J Mater Sci Technol. 2018;34(1):39-57. http://doi.org/10.1016/j.jmst.2017.10.024.
25. Ragu Nathan S, Balasubramanian V, Malarvizhi S, Rao AG. Effect of welding processes on mechanical and microstructural characteristics of high strength low alloy naval grade steel joints. Def Tech. 2015;11(3):308-17. http://doi.org/10.1016/j.dt.2015.06.001.
26. Valdez B, Ramirez J, Eliezer A, Schorr M, Ramos R, Salinas R. Corrosion assessment of infrastructure assets in coastal seas. J Marin Eng Tech. 2016;15(3):124-34. http://doi.org/10.1080/20464177.2016.1247635.
27. Australian Stainless Steel Development Association – ASSDA [homepage on the Internet]. Brisbane: ASSDA; 2025 [cited 2024 Oct 22]. Available from: https://www.assda.asn.au/component/content/article?id=170...in-marine
28. Jafarzadegan M, Feng AH, Abdollah-zadeh A, Saeid T, Shen J, Assadi H. Microstructural characterization in dissimilar friction stir welding between 304 stainless steel and st37 steel. Mater Charact. 2012;74:28-41. http://doi.org/10.1016/j.matchar.2012.09.004.
29. Tiwari A, Singh P, Pankaj P, Biswas P, Kore SD, Pal S. Effect of tool offset and rotational speed in dissimilar friction stir welding of AISI 304 stainless steel and mild steel. J Mater Eng Perform. 2019;28(10):6365-79. http://doi.org/10.1007/s11665-019-04362-y.
30. Das U, Toppo V. Bending strength evaluation of friction stir welded AA6101-T6 and AA6351-T6 aluminium alloys butt joint. Mater Today Proc. 2018;5(5):11556-62. http://doi.org/10.1016/j.matpr.2018.02.123.
31. Daniolos NM, Pantelis DI. Microstructural and mechanical properties of dissimilar friction stir welds between AA6082-T6 and AA7075-T651. Int J Adv Manuf Technol. 2017;88(9-12):2497-505. http://doi.org/10.1007/s00170-016-8965-x.
32. Yan J, Gao M, Zeng X. Study on microstructure and mechanical properties of 304 stainless steel joints by TIG, laser and laser-TIG hybrid welding. Opt Lasers Eng. 2010;48(4):512-7. http://doi.org/10.1016/j.optlaseng.2009.08.009.
33. Park SHC, Sato YS, Kokawa H, Okamoto K, Hirano S, Inagaki M. Microstructural characterisation of stir zone containing residual ferrite in friction stir welded 304 austenitic stainless steel. Sci Technol Weld Join. 2005;10(5):550-6. http://doi.org/10.1179/174329305X46691.
34. Noell PJ, Carroll JD, Boyce BL. The mechanisms of ductile rupture. Acta Mater. 2018;161:83-98. http://doi.org/10.1016/j.actamat.2018.09.006.
35. Dada OJ. Fracture mechanics and mechanical behaviour in AA5083-H111 friction stir welds. Sci Am. 2020;8(1):e00265. http://doi.org/10.1016/j.sciaf.2020.e00265.
36. Akpanyung KV, Loto RT. Pitting corrosion evaluation: a review. J Phys Conf Ser. 2019;1378(2):022088. http://doi.org/10.1088/1742-6596/1378/2/022088.
37. Yi Y, Cho P, Al Zaabi A, Addad Y, Jang C. Potentiodynamic polarization behaviour of AISI type 316 stainless steel in NaCl solution. Corros Sci. 2013;74:92-7. http://doi.org/10.1016/j.corsci.2013.04.028.

Data Availability

The entire dataset supporting the results of this study was published in the article itself.